CHAPTER I-1-A

Principles of Solar Cell Operation

Tom Markvart[1] **and Luis Castañer**[2]
[1]University of Southampton, Southampton, United Kingdom
[2]Universidad Politecnica de Catalunya, Barcelona, Spain

This chapter was previously featured in the 2nd edition and reproduced with minor modifications.

1 INTRODUCTION

Photovoltaic energy conversion in solar cells consists of two essential steps. First, absorption of light generates an electron–hole pair. The electron and hole are then separated by the structure of the device—electrons to the negative terminal and holes to the positive terminal—thus generating electrical power.

This process is illustrated in Fig. 1, which shows the principal features of the typical solar cells in use today. Each cell is depicted in two ways. One diagram shows the physical structure of the device and the dominant electron-transport processes that contribute to the energy-conversion process. The same processes are shown on the band diagram of the semiconductor, or energy levels in the molecular devices.

The diagrams in Fig. 1 are schematic in nature, and a word of warning is in place regarding the differences in scale: whilst the thickness of crystalline silicon cells (shown in Fig. 1A and F) is of the order of 100 μm or more, the thickness of the various devices in Fig. 1B–E (thin-film and GaAs-based cells) might be several micrometers or less. The top surface of the semiconductor structures shown in Fig. 1 would normally be covered with antireflection coating. The figure caption can also be used to locate the specific chapter in this book where full details for each type of device can be found.

McEvoy's Handbook of Photovoltaics.
DOI: http://dx.doi.org/10.1016/B978-0-12-809921-6.00001-X

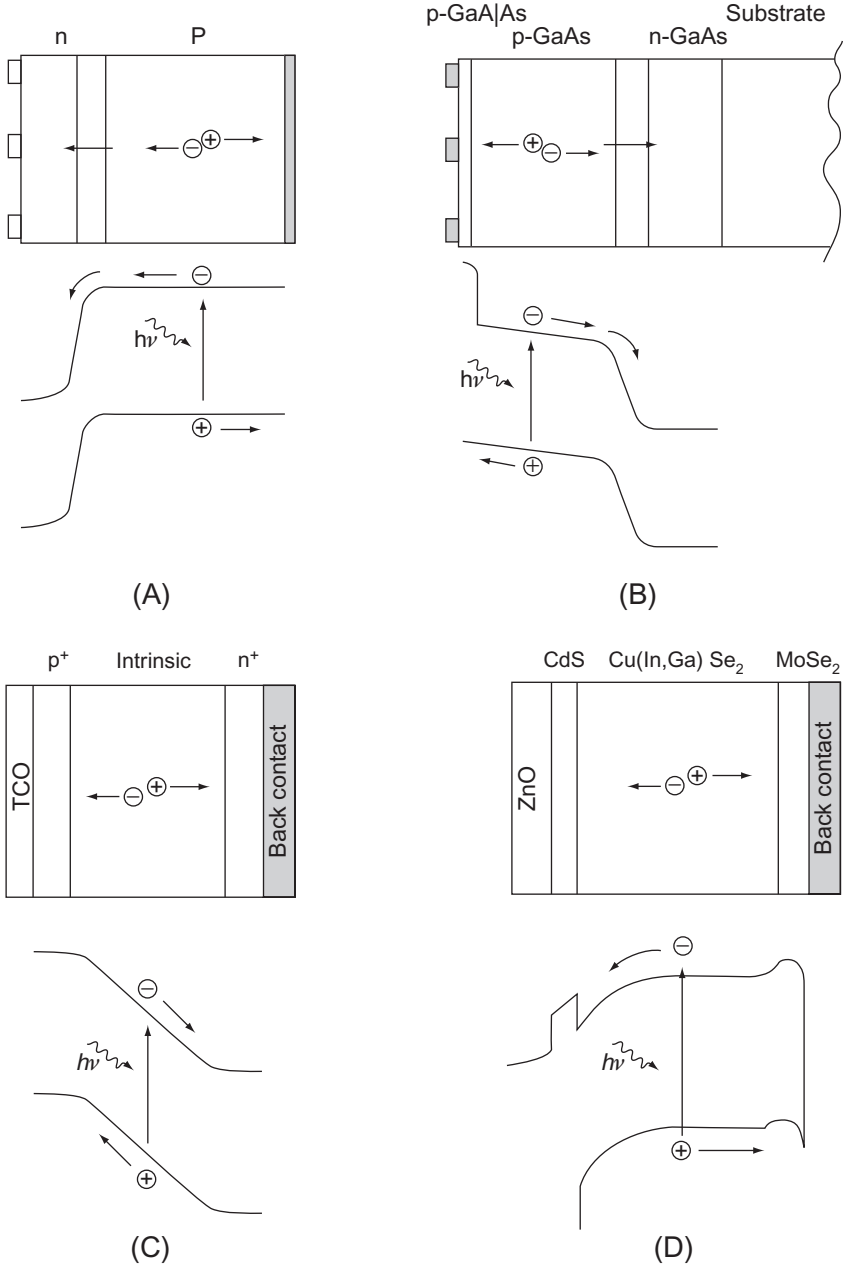

Figure 1 (Continued)

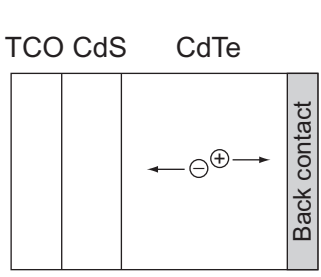

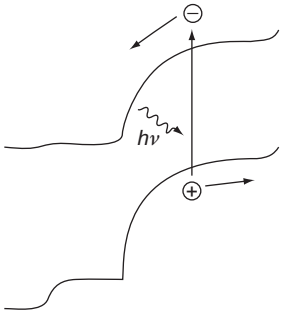

(E)

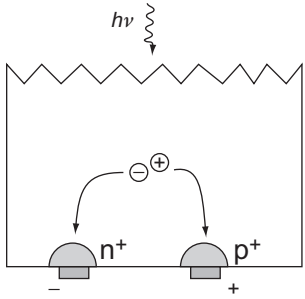

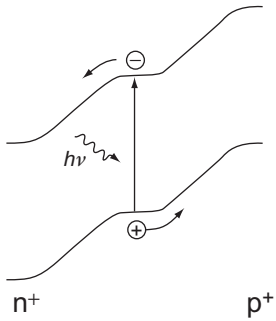

(F)

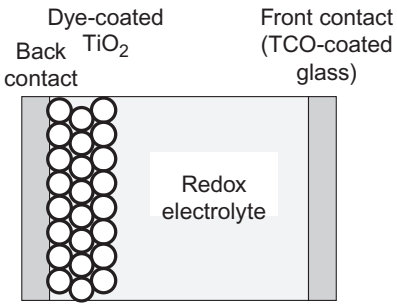

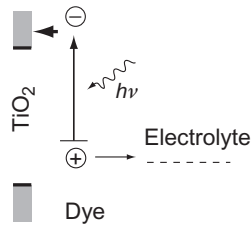

(G)

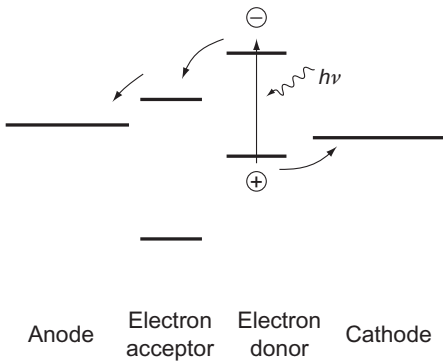

(H)

Figure 1 (Continued)

Figure 1 (A) The structure of crystalline silicon solar cell, the typical solar cell in use today. The bulk of the cell is formed by a thick p-type base in which most of the incident light is absorbed and most power is generated. After light absorption the minority carriers (electrons) diffuse to the junction where they are swept across by the strong built-in electric field. The electrical power is collected by metal contacts to the front and back of the cell (see Chapter I-2-B: High-Efficiency Silicon Solar Cell Concepts and Chapter I-2-C: Low-Cost Industrial Technologies for Crystalline Silicon Solar Cells). (B) The typical gallium–arsenide solar cell has what is sometimes called a heteroface structure, by virtue of the thin passivating GaAlAs layer that covers the top surface. The GaAlAs "window" layer prevents minority carriers from the emitter (electrons) to reach the surface and recombine but transmits most of the incident light into the emitter layer where most of the power is generated. The operation of this p–n junction solar cell is similar in many respects to the operation of the crystalline silicon solar cell in (A), but the substantial difference in thickness should be noted (see Chapter I-4-A: GaAs and High-Efficiency Space Cells and Chapter I-4-B: High-Efficiency III-V Multijunction Solar Cells). (C) The structure of a typical single-junction amorphous silicon solar cells. Based on p–i–n junction, this cell contains a layer of intrinsic semiconductor that separates two heavily doped p and n regions near the contacts. Generation of electrons and holes occurs principally within the space-charge region, with the advantage that charge separation can be assisted by the built-in electric field, thus enhancing the collection efficiency. The contacts are usually formed by a *transparent conducting oxide* (TCO) at the top of the cell and a metal contact at the back. Light-trapping features in TCO can help reduce the thickness and reduce degradation. The thickness of a-Si solar cells ranges typically from a fraction of a micrometer to several micrometers (see Chapter I-3-A: Thin-Film Silicon Solar Cells). (D) and (E) The typical structures of solar cells based on compound semiconductors copper indium–gallium diselenide (D) and cadmium telluride (E). The front part of the junction is formed by a wide-band-gap material (CdS "window") that transmits most of the incident light to the absorber layer ($Cu(In,Ga)Se_2$ or CdTe) where virtually all electron–hole pairs are produced. The top contact is formed by a TCO. These solar cells are typically a few micrometers thick (see Chapter I-3-B: Alessandro Romeo, and Chapter I-3-C: Cu(In,Ga)Se2 Thin-Film Solar Cells). (F) Contacts can be arranged on the same side of the solar cell, as in this point contact solar cell. The electron–hole pairs are generated in the bulk of this crystalline silicon cell, which is near intrinsic, usually slightly n-type. Slightly thinner than the usual crystalline silicon solar cell, efficient light absorption is aided here by light trapping: a textured top surface and a reflecting back surface (see Chapter I-2-C: Low-Cost Industrial Technologies for Crystalline Silicon Solar Cells). (G) and (H) The most recent types of solar cell are based on molecular materials. In these cells, light is absorbed by a dye molecule, transferring an electron from the ground state to an excited state rather than from the valence band to the conduction band as in the semiconductor cells. The electron is subsequently removed to an electron acceptor and the electron deficiency (hole) in the ground state is replenished from an electron donor. A number of choices exist for the electron acceptor and donor. In the dye-sensitized cell (G, see Chapter I-5-A: Dye-Sensitized Photoelectrochemical Cells), the electron donor is a redox electrolyte and the role of electron acceptor is the conduction band of titanium dioxide. In plastic solar cells (H, see Chapter I-5-B: Organic Solar Cells), both electron donor and electron acceptor are molecular materials.

2 ELECTRICAL CHARACTERISTICS

2.1 The ideal solar cell

An ideal solar cell can be represented by a current source connected in parallel with a rectifying diode, as shown in the equivalent circuit of Fig. 2. The corresponding $I-V$ characteristic is described by the Shockley solar cell equation

$$I = I_{\mathrm{ph}} - I_{\mathrm{o}}\left(e^{\frac{qV}{k_{\mathrm{B}}T}} - 1\right) \tag{1}$$

where k_{B} is the Boltzmann constant, T is the absolute temperature, q (>0) is the electron charge, and V is the voltage at the terminals of the cell. I_{o} is well known to electronic device engineers as the diode saturation current (see, for example, [1]), serving as a reminder that a solar cell in the dark is simply a semiconductor current rectifier, or diode. The photogenerated current I_{ph} is closely related to the photon flux incident on the cell, and its dependence on the wavelength of light is frequently discussed in terms of the quantum efficiency or spectral response (see Section 2.3). The photogenerated current is usually independent of the applied voltage with possible exceptions in the case of a-Si and some other thin-film materials [2–4].

Fig. 3A shows the $I-V$ characteristic (Eq. (1)). In the ideal case the short-circuit current I_{sc} is equal to the photogenerated current I_{ph}, and the open-circuit voltage V_{oc} is given by

$$V_{\mathrm{oc}} = \frac{k_{\mathrm{B}}T}{q}\ln\left(1 + \frac{I_{\mathrm{ph}}}{I_0}\right) \tag{2}$$

The maximum theoretically achievable values of the short-circuit current density J_{ph} and of the open-circuit voltage for different materials are discussed and compared with the best measured values in Chapter I-1-C, Ideal Efficiencies.

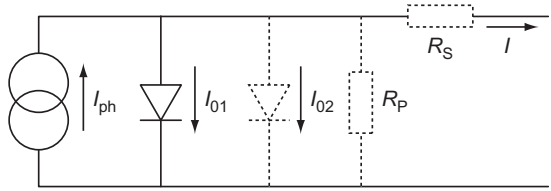

Figure 2 The equivalent circuit of an ideal solar cell (full lines). Nonideal components are shown by the dotted line.

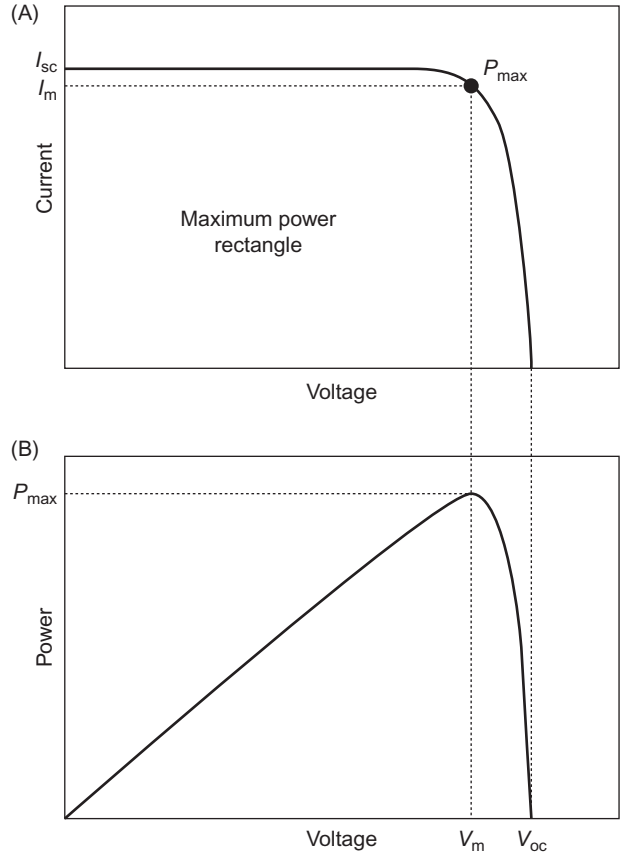

Figure 3 The $I-V$ characteristic of an ideal solar cell (A) and the power produced by the cell (B). The power generated at the maximum power point is equal to the shaded rectangle in (A).

The power $P = IV$ produced by the cell is shown in Fig. 3B. The cell generates the maximum power $P_{\rm max}$ at a voltage $V_{\rm m}$ and current $I_{\rm m}$, and it is convenient to define the fill factor FF by

$$\mathrm{FF} = \frac{I_{\rm m} V_{\rm m}}{I_{\rm sc} V_{\rm oc}} = \frac{P_{\rm max}}{I_{\rm sc} V_{\rm oc}} \tag{3}$$

The fill factor FF of a solar cell with the ideal characteristic (1) will be furnished by the subscript 0. It cannot be determined analytically, but it can be shown that FF_0 depends only on the ratio $\nu_{\rm oc} = V_{\rm oc}/k_{\rm B}T$. FF_0 is determined, to an excellent accuracy, by the approximate expression [5]

$$\mathrm{FF}_0 = \frac{\nu_{\rm oc} - \ln\left(\nu_{\rm oc} + 0.72\right)}{\nu_{\rm oc} + 1}$$

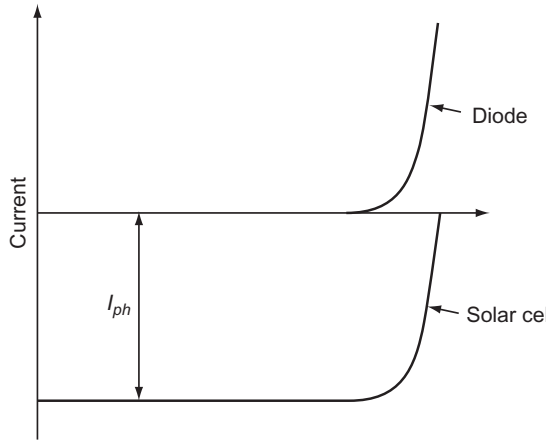

Figure 4 The superposition principle for solar cells.

The $I-V$ characteristics of an ideal solar cell complies with the *superposition principle*: the functional dependence (1) can be obtained from the corresponding characteristic of a diode in the dark by shifting the diode characteristic along the current axis by I_{ph} (Fig. 4).

2.2 Solar cell characteristics in practice

The $I-V$ characteristic of a solar cell in practice usually differs to some extent from the ideal characteristic (1). A two-diode model is often used to fit an observed curve, with the second diode containing an "ideality factor" of 2 in the denominator of the argument of the exponential term. The solar cell (or circuit) may also contain series (R_{s}) and parallel (or shunt, R_{p}) resistances, leading to a characteristic of the form

$$= I_{\mathrm{ph}} - I_{\mathrm{o1}}\left\{\exp\left(\frac{V+IR_{\mathrm{s}}}{k_{\mathrm{B}}T}\right)\right\} - I_{\mathrm{o2}}\left\{\exp\left(\frac{V+IR_{\mathrm{s}}}{2k_{\mathrm{B}}T}\right) - 1 - \frac{V+IR_{\mathrm{S}}}{R_{\mathrm{p}}}\right\} \tag{4}$$

where the light-generated current I_{ph} may, in some instances, depend on the voltage, as we have already noted. These features are shown in the equivalent circuit of Fig. 2 by the dotted lines. The effect of the second diode, and of the series and parallel resistances, on the $I-V$ characteristic of the solar cell is shown in Figs. 5 and 6, respectively; further information about these parameters can be obtained from the dark characteristic (Fig. 7). The effect of the series resistance on the fill factor can be allowed for by writing where $rs = R_{\mathrm{s}}I_{\mathrm{sc}}/V_{\mathrm{oc}}$. An analogous expression exists also

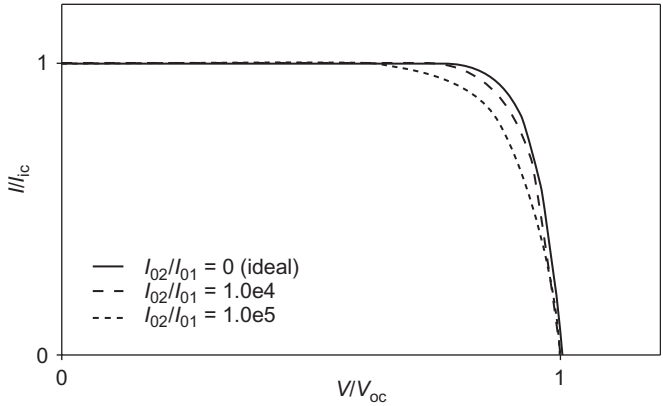

Figure 5 The $I-V$ characteristic of the solar cell in the two-diode model for three values of the ratio I_{02}/I_{01}.

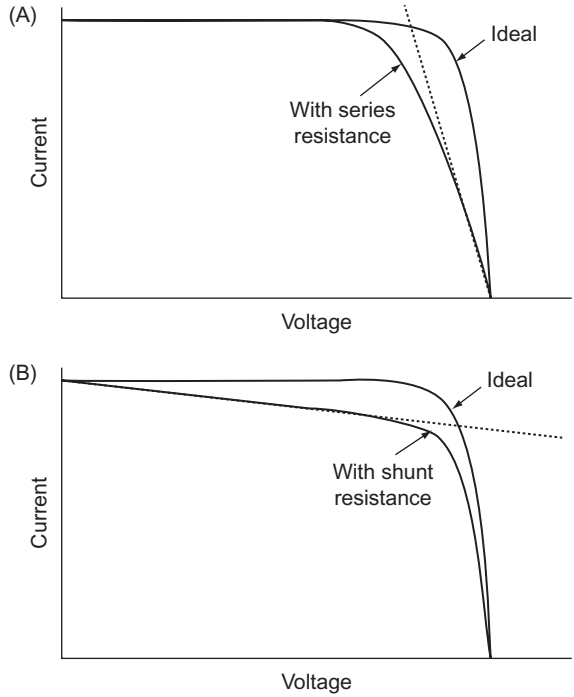

Figure 6 The effect of series (A) and parallel (B) resistance on the $I-V$ characteristic of the solar cell.

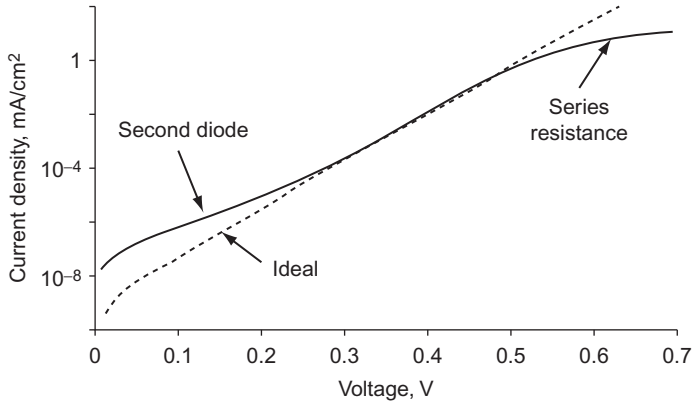

Figure 7 The dark *I–V* characteristic of a solar cell for the two-diode model including the series resistance. The shunt resistance has a similar effect to the second diode.

for the parallel resistance. Instead of the two-diode Eq. (4), an empirical nonideality factor *nid* can be introduced in the single-diode Eq. (1) that usually lies between 1 and 2. Two among a number of possible sources of nonideal behavior—recombination in the depletion region and the series resistance—are discussed in Sections 4.1 and 4.4.

$$\mathrm{FF} = \mathrm{FF}_0(1 - r_s) \tag{5}$$

2.3 The quantum efficiency and spectral response

The quantum efficiency of a solar cell is defined as the ratio of the number of electrons in the external circuit produced by an incident photon of a given wavelength. Thus one can define external and internal quantum efficiencies (denoted by EQE(λ) and IQE(λ), respectively). They differ in the treatment of photons reflected from the cell: all photons impinging on the cell surface are taken into account in the value of the EQE but only photons that are not reflected are considered in the value of IQE.

If the internal quantum efficiency is known, the total photogenerated current is given by

$$I_{\mathrm{ph}} = q \int_{(\lambda)}^{\Phi} (\lambda)\{1 - R(\lambda)\}\ \mathrm{IQE}\ (\lambda) d\lambda \tag{6}$$

where $\Phi(\lambda)$ is the photon flux incident on the cell at wavelength λ, $R(\lambda)$ is the reflection coefficient from the top surface (see Section 3.1), and the

integration is carried out over all wavelength λ of light absorbed by the solar cell. The values of the IQE and EQE are routinely measured to assess the performance of a solar cell by using interference filters or monochromators.

The *spectral response* (denoted by SR(λ), with the units A/W) is defined as the ratio of the photocurrent generated by a solar cell under monochromatic illumination of a given wavelength to the value of the spectral irradiance at the same wavelength. Since the number of photons and irradiance are related, the spectral response can be written in terms of the quantum efficiency as (see, for instance [6])

$$\mathrm{SR}(\lambda) = \frac{q\lambda}{hc}\mathrm{QE}(\lambda) = 0.808 \cdot \lambda \cdot \mathrm{QE}(\lambda) \tag{7}$$

where λ is in micrometers. Spectral response in (7) can be either internal or external, depending on which value is used for the quantum efficiency.

3 OPTICAL PROPERTIES

3.1 The antireflection coating

Most solar cells rely on a thin layer of a dielectric (an antireflection coating) to reduce the reflection of light from the front surface of the cell. This section gives a brief description of the reflection of light from a bare semiconductor, and from a semiconductor with a single-layer antireflection coating. The discussion is confined to the case of normal incidence of light onto a smooth planar surface.

The reflection coefficient from bare silicon for light incident from air is given by

$$R = \frac{(\mathbf{n}-1)^2 + k^2}{(\mathbf{n}+1)^2 + k^2} \tag{8}$$

where $\mathbf{n}$ and k are the refractive index and the extinction coefficient of the semiconductor, both in general functions of the wavelength λ of light in vacuum. The extinction coefficient is related to the absorption coefficient α by

$$k = \frac{\alpha\lambda}{4\pi\mathbf{n}} \tag{9}$$

For single-layer antireflection coating of refractive index $\mathbf{n}_{ar}$ between a top medium of refractive index $\mathbf{n}_0$ (for example, glass or air) and a semiconductor, the reflection coefficient becomes, neglecting light absorption in the semiconductor

$$R = \frac{r_0^2 + r_{sc}^2 + 2r_0 r_{sc}\cos 2\beta}{1 + r_0^2 + 2r_0 r_{sc}\cos 2\beta} \tag{10}$$

where

$$r_0 = \frac{\mathbf{n}_{ar} - \mathbf{n}_0}{\mathbf{n}_{ar} + \mathbf{n}_0}; \quad r_{sc} = \frac{\mathbf{n}_{sc} - \mathbf{n}_{ar}}{\mathbf{n}_{sc} + \mathbf{n}_{ar}} \qquad \beta = \frac{2\pi}{\lambda}\mathbf{n}_{ar} d$$

and d denotes the thickness of the coating. The transmission coefficient is, in both cases, simply

$$T = 1 - R \tag{11}$$

In most cases of interest, both r_{sc} and r_0 are positive and R vanishes when

$$d = \frac{\lambda}{4\mathbf{n}_{ar}}; \frac{3\lambda}{4\mathbf{n}_{ar}}; \frac{5\lambda}{4\mathbf{n}_{ar}}, \ldots \tag{12}$$

and

$$\mathbf{n}_{ar} = \sqrt{\mathbf{n}_0 \mathbf{n}_{sc}} \tag{13}$$

The first value of d in Eq. (12) is often used in practice under the name of *quarter-wavelength rule* since $\lambda/\mathbf{n}_{ar}$ is the wavelength of light in the antireflection coating.

Reflection from the top surface can be reduced further by the use of a multilayer coating. The details of such coatings as well as a general theory for an oblique incidence of light can be found, for example, in [7]. Fig. 8 compares the reflection coefficients for a smooth bare silicon surface, a smooth surface covered with antireflection coating, and a textured surface with antireflection coating.

3.2 Light trapping

In solar cells with a simple geometry, light rays enter the cell through the front surface and, if not absorbed, leave through the rear surface of the cell. More sophisticated arrangements exist that extend the path of light inside the cell, and they are usually referred to as *optical confinement* or *light*

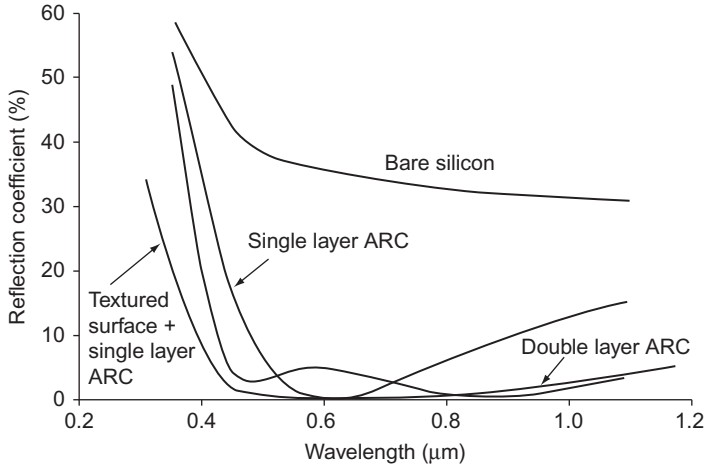

Figure 8 The reflection coefficient from polished bare silicon and a polished silicon surface covered with a single- and double-layer antireflection coating. *After K. Zweibel, P. Hersch, Basic Photovoltaic Principles and Methods, Van Nostrand Reinhold, New York, 1984; A. Goetzberger, J. Knobloch, B. Voss, Crystalline Silicon Solar Cells, John Wiley & Sons, Chichester, 1998. The reflection coefficient for a textured surface is also shown.*

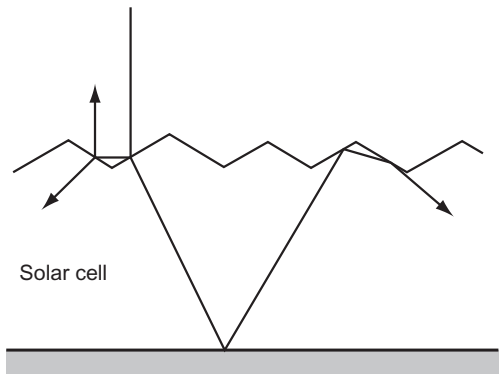

Figure 9 The textured top surface reduces reflection from the solar cell and, when combined with a reflecting back surface, helps to confine or "trap" light within the cell.

trapping. In crystalline or amorphous silicon solar cells, light trapping is used to reduce the thickness of the cell without lowering the light absorption within the cell. Light trapping can also be used to enhance the open-circuit voltage [10,11].

The most common light-trapping features include a textured top surface combined with an optically reflecting back surface (Fig. 9).

In the ideal case, Yablonovich [12] and Yablonovich and Cody [13] (see also Miñano [14]) has shown that a randomly textured (so-called Lambertian) top surface in combination with a perfect back-surface reflector produces a light-trapping scheme that enhances the light intensity inside the cell by a factor of $\mathbf{n}_{sc}^2$ where, as in Section 3.1, $\mathbf{n}_{sc}$ is the refractive index of the solar cell material. This arrangement also increases the average path length of light rays inside the cell from $2W$, in the case of single pass through the cell, to $4\mathbf{n}_{sc}^2 W$ in the case of complete light trapping, where W the cell thickness. Schemes have been developed to enhance the operation of practical devices including crystalline, polycrystalline, and amorphous silicon cells (discussed in Chapter I-2-B, High-Efficiency Silicon Solar Cell Concepts, Chapter I-2-C, Low-Cost Industrial Technologies for Crystalline Silicon Solar Cells, Chapter I-2-D, Thin Crystalline and Polycrystalline Silicon Solar Cells, and Chapter I-3-A, Thin-Film Silicon Solar Cells). With application to the latter cells, Schropp and Zeman [15] consider the trapping and scattering of light at rough interfaces in some detail. In gallium–arsenide cells, multilayer Bragg reflectors (in place of the back-surface reflector) have been used with success (see Chapter I-4-A: GaAs and High-Efficiency Space Cells).

4 TYPICAL SOLAR CELL STRUCTURES

4.1 The p–n junction solar cell

The planar p–n junction solar cell under low injection is usually singled out for special analysis since realistic approximations exist that allow analytic solutions to be developed and used successfully for the description of practical devices. The success of this model is due, to a large extent, to the clear way the cell can be divided into three regions—emitter, junction region, and base—that serve a different purpose in solar cell operation.

The emitter and the base—which remain largely neutral during the cell operation—absorb the main part of the incident light and transport the photogenerated minority carriers to the junction. The p–n junction—which contains a strong electric field and a fixed space charge—separates the minority carriers that are collected from the emitter and

the base. The junction is effectively devoid of mobile charge carriers and is sometimes called the *depletion region*.

4.1.1 The p–n junction

Fig. 10 shows the principal parameters of a p–n junction in equilibrium along the spatial coordinate perpendicular to the junction. In operation the Fermi-level EF splits into two quasi-Fermi levels EF_n and EFp, one each for the electrons and the holes, with the corresponding potentials $\phi n = -q/\mathrm{EF}n$ and $\phi \mathrm{p} = -q/\mathrm{EFp}$. Near the open circuit the quasi-Fermi levels are parallel in the junction, their gradients are small, and their splitting is equal to the observed voltage at the junction (Fig. 11). The charge carrier statistics in terms of the quasi-Fermi levels is discussed in Section 3 of Chapter I-1-B, Semiconductor Materials and Modeling.

Under illumination or under applied bias in the dark the electrostatic potential difference $\Delta\psi$ between the two sides of the junction is a difference of two terms: the equilibrium built-in voltage V_{bi} and the voltage V at the junction edges

$$\Delta\psi = V_{\mathrm{bi}} - V \tag{14}$$

$$qV_{\mathrm{bi}} = k_{\mathrm{B}}T \ \ln\left(\frac{N_{\mathrm{D}}N_{\mathrm{A}}}{N_{\mathrm{i}}^2}\right) \tag{15}$$

where N_{A} and N_{D} are the acceptor and the donor concentrations on the p- and n-sides of the junction, respectively. In the absence of resistive losses, V is equal to the voltage measured at the terminals of the cell. The junction width W_{j} is given by

$$W_{\mathrm{j}} = L_{\mathrm{D}}\sqrt{\frac{2q\Delta\psi}{k_{\mathrm{B}}T}} \tag{16}$$

Here, L_{D} is the Debye length

$$L_{\mathrm{D}} = \frac{\sqrt{\varepsilon k_{\mathrm{B}}T}}{q^2 N_{\mathrm{B}}} \tag{17}$$

where ε is the static dielectric constant, and

$$N_{\mathrm{B}} = \frac{N_{\mathrm{A}}N_{\mathrm{D}}}{N_{\mathrm{A}} + N_{\mathrm{D}}}$$

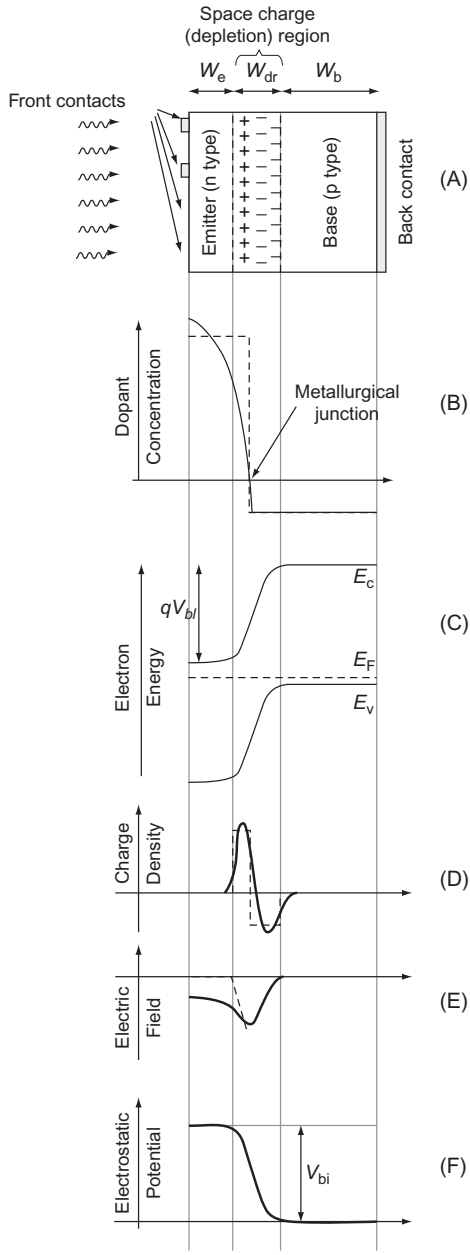

Figure 10 The p−n junction solar cell in equilibrium. (A) The physical layout (not to scale); (B) the difference of dopant concentrations $ND - NA$; (C) the band diagram; (D) charge density; (E) electric field; (F) electrostatic potential. The quantities shown by the dashed line correspond to an idealized abrupt junction with constant dopant concentrations in the base and in the emitter; the full line corresponds to a typical industrial solar cell with a diffused emitter.

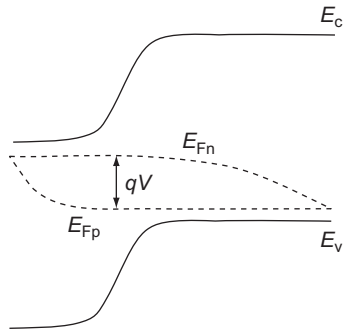

Figure 11 The p–n junction at open circuit.

In an ideal p–n junction solar cell the junction (or depletion) region serves as a lossless mechanism for extracting and separating the minority carriers from the quasi-neutral regions—the base and the emitter. The function of the junction can then be summarized in the form of boundary conditions that link the majority carrier concentration on one side of the junction with the minority-carrier concentration on the other. For an n-type emitter and a p-type base, for example, the following relations hold:

$$n(\text{base}) = n_0(\text{base})e^{qV/k_B T} = n_0(\text{emitter})e^{q(V-V_{bi})/k_B T} \tag{18}$$

Eq. (18) relates the electron concentration n(base) at the edge of the depletion region of the base to its equilibrium value n_0(base) and to the equilibrium electron concentration n_0(emitter) at junction edge of the emitter. A similar relationship exists for the hole concentration at the junction edge of the emitter and the base:

$$p(\text{emitter}) = p_0(\text{emitter})e^{qV/k_B T} = p_0(\text{base})e^{q(V-V_{bi})/k_B T} \tag{19}$$

Eqs. (18) and (19) are the boundary conditions for an analytical solution of the transport equations (discussed in Chapter I-1-B, Semiconductor Materials and Modeling, Section 4) in the quasi-neutral regions. A rigorous discussion of this *depletion approximation* which forms the basis for the analytical treatment, can be found in Ref. [16].

The photogenerated and dark saturation currents for the cell are obtained by adding the relevant quantities for the base and the emitter:

$$\begin{aligned} I_{ph} &= I_{phb} + I_{phe} \\ I_0 &= I_{0b} + I_{0e} \end{aligned} \tag{20}$$

A similar result holds also for the quantum efficiency. It is sometimes convenient to define the collection efficiency ϑi for a region i (where i stands for the base, the emitter, or the depletion region) as the probability that an electron–hole pair generated in this region reaches the junction

$$\mathrm{EQE}_i(\lambda) = a_1(\lambda)\vartheta_1(\lambda) \tag{21}$$

where $ai(\lambda)$ is the (fractional) number of electron–hole pairs generated by each photon of incident light in region i.

No recombination occurs in an ideal p–n junction, but the (small) light-generated current produced here can be added to the first Eq. (20). Recombination is included in more realistic analytical theories: the original treatment by Sah et al. [17] uses the Shockley–Read–Hall model of recombination via defects (see Chapter I-1-B, Semiconductor Materials and Modeling, Section 7) with the principal result that the current in (I) is reduced by a term of the form

$$I_{02}\left(e^{\frac{qV}{2K_\mathrm{B}T}} - 1\right) \tag{22}$$

In other words, recombination in the depletion region gives rise to an additional dark current corresponding to the second diode in the I–V characteristic (4), as already discussed in Section 2.2.

4.1.2 Uniform emitter and base

Analytical expressions for the photogenerated and dark saturation current densities for the emitter or base can be obtained if the dopant concentration and all other parameters are assumed constant. To this end, we define

$$\zeta = \frac{SL}{D} \tag{23}$$

$$\gamma_+ = (\zeta + 1)e^{W/L} + (\zeta - 1)e^{-W/L} \tag{24}$$

$$\gamma_- = (\zeta + 1)e^{W/L} - (\zeta - 1)e^{-W/L} \tag{25}$$

where S is the surface recombination velocity at external surface (front surface in the case of emitter and rear surface in the case of base); W is the width of the relevant region (W_e for the emitter and W_b for the base); and $L = \sqrt{D\tau}$ is the minority-carrier diffusion length, where τ is the minority-carrier lifetime, and D is the minority-carrier diffusion

Table 1 The internal quantum efficiency (IQE) for the emitter and the base in the uniform doping model. The subscripts *e* or *b* of γ, ζ, *L*, and *W* refers to the emitter or base, respectively. In the case of base, IQE is understood per unit photon entering from the junction

	IQE(λ)
Base	$\frac{\alpha L_b}{\gamma b -}\left\{\frac{\zeta_b+1}{1+\alpha L_b}(e^{W_b/L_b}-e^{-\alpha W_b})+\frac{\zeta_b-1}{1-\alpha L_b}(e^{-W_b/L_b}-e^{-\alpha W_b})\right\}$ $\rightarrow \frac{\alpha L_b}{1+\alpha L_b}$ for an infinite base $(W_b \rightarrow \infty)$
Emitter	$***\frac{\alpha L_b e^{-aW_e}}{\gamma_{e^-}}\left\{\frac{\zeta_e+1}{1+\alpha L_e}(e^{-W_e/L_e}-e^{+\alpha W_e})+\frac{\zeta_e-1}{1-\alpha L_e}(e^{+W_e/L_e}-e^{+\alpha W_e})\right\}***$

constant. The photogenerated and dark saturation currents for each region are then given by

$$J_0 = \frac{qD}{L}\frac{n_i^2}{N_{\text{dop}}}\frac{\gamma_+}{\gamma_-} \tag{26}$$

where N_{dop} is the dopant concentration *NA* or *ND* appropriate for the relevant region. The internal quantum efficiency for each region is given in Table 1.

4.1.3 Diffused emitter

In practical silicon solar cells the emitter is generally fabricated by diffusion of impurities into the semiconductor wafer. This creates a thin layer where the impurity gradient is very high and the approximation of constant doping concentration does not hold. Simultaneously the continuity and current equations do not combine into a second-order differential equation with constant coefficients, and a simple analytical solution cannot be found. Several approaches have been followed besides the numerical integration of the equations [18] to reach a reasonably simple analytical or truncated series solutions. Analytical solutions were reviewed in Ref. [19], where the errors have been estimated for the transparent emitter [20] and the quasi-transparent emitter [21] solutions. An emitter is considered transparent when the recombination inside the emitter bulk is negligible and quasi-transparent when this recombination can be considered as a perturbation to the transparent solution. Solutions based on an infinite series that can be truncated to provide different order approximations were proposed in Ref. [22] and were extended as a succession of asymptotic expansions

in [23]. One of the simplest yet accurate solutions is given in Alcubilla et al. [24] based on the superposition of zero-input and zero-state solutions of the continuity equation with a boundary condition at the surface given by a surface recombination velocity S as follows:

$$J_0 = \frac{qn_i^2}{\int_0^{W_e} \frac{N_{\text{eff}}}{D}\,dx + \frac{N_{\text{eff}}(W_e)}{S}} + qn_i^2 \int_0^{W_e} \frac{dx}{N_{\text{eff}}\tau} \tag{27}$$

where $N_{\text{eff}}(x)$ is the effective doping concentration at depth x taking into account the effect of band-gap narrowing. A systematic and general formulation of the several approximations is given in Cuevas et al. [25]. An elegant formalism to deal with inhomogeneously doped emitters can be found in del Alamo and Swanson [26].

When the emitter in illuminated, the problem can be solved using the same approaches as used in the dark, computing the emitter collection efficiency ϑem equal, as in Eq. (21), to the ratio of the photogenerated current at the emitter boundary of the space charge region divided by the integrated carrier generation in the emitter. Bisschop et al. [27] extended Park's solution in the dark [22] to illuminated emitters. Cuevas et al. [25] provided a formulation in terms of a series expansion and Alcubilla et al. extended the dark superposition model [24]. The first-order result for the photocurrent is given by (see, for instance [25])

$$J_{\text{ph}} = \frac{q\int_0^{W_e} g(x)dx}{1 + \frac{S}{N_{\text{eff}}(W_e)}\int_0^{W_e} \frac{N_{\text{eff}}}{D}\,dx + \frac{N_{\text{eff}}(W_e)}{S}} \tag{28}$$

where $g(x)$ is the generation rate (see Chapter I-1-B, Semiconductor Materials and Modeling, Section 6.1).

4.2 Heterojunction cells

Heterostructures represent an opportunity to manufacture efficient solar cells from highly absorbing thin-film materials without substantial losses through electron–hole recombination at the front surface. This is illustrated by the structures of the CdS/CdTe and CdS/CIGS solar cells where a wide-band-gap semiconductor (here, CdS) serves as a "window" partner to a lower-band-gap "absorber" where most of the power is generated.

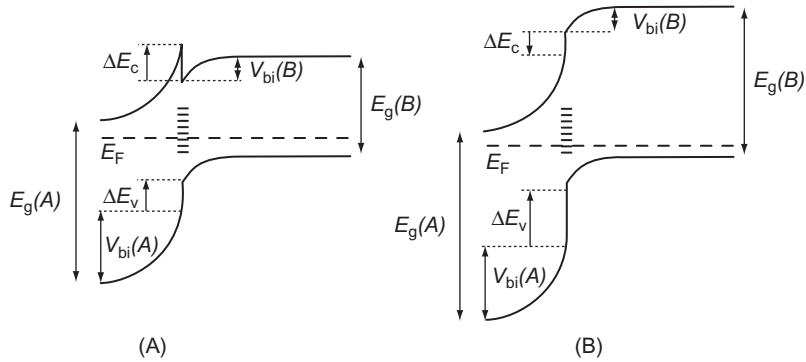

Figure 12 The band diagrams of typical heterojunction solar cells consisting of a window layer of wide-gap n-type semiconductor A, and an absorber of p-type semiconductor B. The energy levels of an interface defect layer and the band-bending potential V_{bi} (A) and V_{bi} (B) are also shown. A spike in the conduction band occurs for positive ΔE_c, as shown in the structure (A).

An important consideration in the heterojunction design includes the band-gap lineups at the interface between the two semiconductors. Fig. 12 shows the equilibrium band diagrams of typical heterojunctions between a wide-gap window A and an absorber B. The band diagram corresponds the usual situation encountered in CdTe and CIGS solar cells where an n-type wide-gap window and a p-type emitter are the most common arrangements. Similarly to the p—n junction the built-in potentials V_{bi}(A) and V_{bi}(B) on the two sides of the junction can be determined by solution of the Poisson equation (see Eq. (7) in Chapter I-1-B, Semiconductor Materials and Modeling). The band-gap discontinuities ΔE_c and ΔE_v have been subject to much discussion over the years, and a number of theories have evolved that provide an understanding in terms of electron affinities and the electron dipole moments at the interface. The discontinuity in the conduction band edge, for example, can be written in the form

$$\Delta E_c = \chi_B - \chi_A + \text{interface dipole terms}$$

where χ_A and χ_B are the electron affinities of semiconductors A and B [28]. The classical Shockley—Anderson model [29] neglects the interface dipole terms. Its limited validity has been discussed extensively (see, for example [30]), although it does seem to provide a reasonable description for some heterojunctions (Fig. 13). In the application to solar cells a full understanding of the problem is hindered further by the

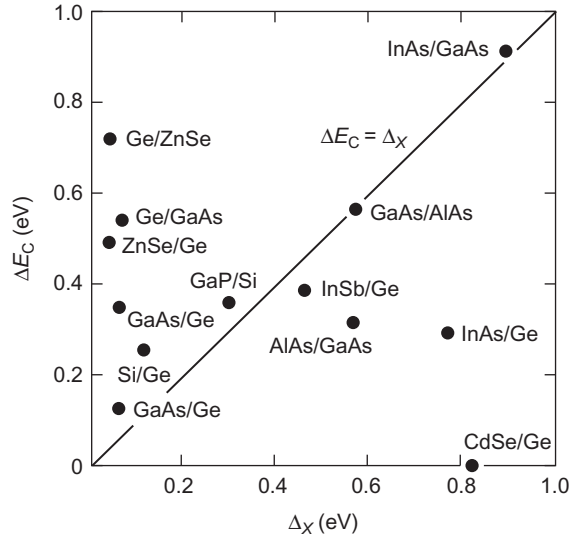

Figure 13 The conduction band discontinuity ΔE_c and the difference of electron affinities $\Delta\chi$ for a number of heterojunctions. *L.J. Brillson, Surfaces and interfaces: atomic-scale structure, band bending and band offsets, in: P.T. Landsberg (Ed.), Handbook of Semiconductors, vol. 1, Elsevier, Amsterdam, 1992, pp. 281–417, p. 391.*

polycrystalline nature of the materials and frequently the presence of more than two layers that need to be considered in the analysis.

On account of the wide band-gap and the weak generation in the window material, both the dark and photogenerated currents from the emitter are significantly smaller that the corresponding quantities from the base. In addition, dark current may contain a component due to recombination at the interface defect states; less frequently, these states also reduce the collection probability and the photogenerated current.

Because of the short minority-carrier diffusion lengths, it is desirable to ensure that minority carriers are generated predominantly in a region where electric field assists collection through drift rather than diffusion. As in the homojunction cell, this can be achieved by employing sufficiently low doping concentrations in the absorber to obtain a wide depletion region; a similar philosophy is also employed in amorphous silicon solar cells, as discussed in Section 4.3 and Chapter I-3-A, Thin-Film Silicon Solar Cells. More detailed description of heterojunctions in application to practical solar cells will be found in Chapter I-3-B, CdTe Solar Cells, and Chapter I-3-C, Cu(In,Ga)Se2 Thin-Film Solar Cells.

Somewhat similar to heterojunction is the *heteroface* solar cell a common structure in GaAs solar cells where a thin layer of wide-gap GaAlAs is deposited to reduce recombination at the top surface. It is more convenient, however, to describe this structure as a homojunction cell with surface passivation that can be treated by the methods described in Section 4.1.

4.3 The p–i–n structure

The analysis of p–i–n junction solar cells is of considerable importance for the understanding of operation of amorphous silicon solar cells. Furthermore, similar principles have been invoked in the description of other thin-film solar cells where the carrier diffusion is ineffective and the electric field is used to enhance carrier transport and collection. Despite this importance, however, the theoretical understanding of these structures is limited, hampered by the fundamental complexity of the problem. Indeed the less-than-complete knowledge of the parameters of amorphous or polycrystalline material is compounded by mathematical difficulties arising principally from the need to solve the nonlinear transport equations. Although a detailed description is possible only with the use of numerical computational techniques, a broad understanding can be gained through judicious approximations based on a physical insight [31].

A schematic band diagram of a p–i–n structure is shown in Fig. 14. Noting that the carrier transport dominant chiefly by drift in the electric

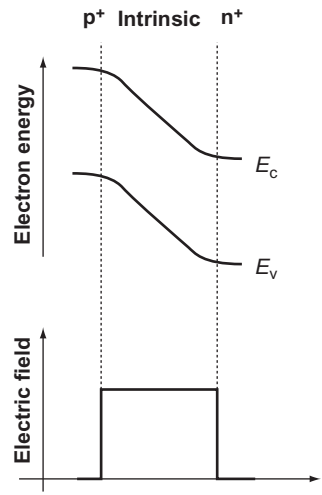

Figure 14 An idealized model of a p–i–n junction amorphous silicon solar cell with a constant electric field in the intrinsic region.

field of the junction rather than by diffusion, carrier collection will be described by the drift lengths l_n and l_p rather than by the diffusion lengths L_n and L_p (see Chapter I-1-B: Semiconductor Materials and Modeling, Section 7.3). The recombination can be conveniently approximated with the use of minority-carrier lifetimes τ_n and τ_p on the two sides of the junction where electrons and holes are minority carriers, respectively. The use of constant electric field ε is obviously an approximation, but it is usually a good one if carrier injection is not too high. A reasonably simple analysis is then possible that, in the limit of weak absorption, results in an analytical expression in the form

$$J = qg\ell_c(1 - e^{-W_1/\ell_c}) \tag{29}$$

for the current density produced by illumination. In Eq. (29), Wi is the width of the intrinsic region, and

$$\ell_c = \ell_n + \ell_p \tag{30}$$

is the collection length, d is the width of the i layer, and g is the generation function, which is assumed here to be constant. Equations similar to (29) have been used with success to interpret various characteristics of p–i–n solar cells (see, for example [4]).

An extension of this theory was later proposed that allows for the three charge states of the dangling bonds in amorphous silicon rather than

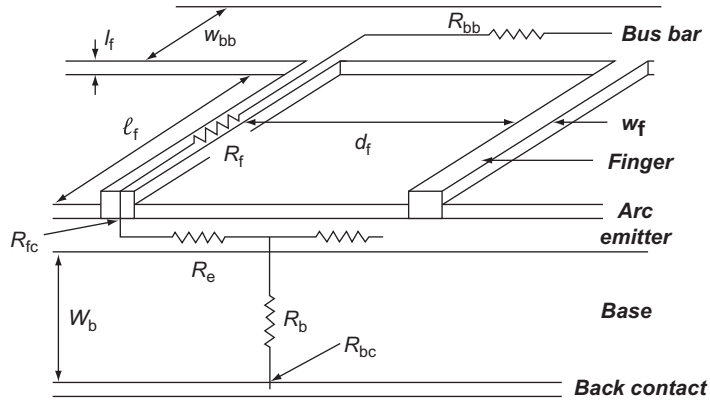

Figure 15 Components of the series resistance in a p–n junction solar cell. *After R. van Overstraeten, R.P. Mertens, Physics, Technology and Use of Photovoltaics, Adam Hilger, Bristol, 1986; A. Goetzberger, J. Knobloch, B. Voss, Crystalline Silicon Solar Cells, John Wiley & Sons, Chichester, 1998.*

Table 2 Expressions for the various components of the series resistance; the bus-bar resistance assumes that connection is made at one end. Here, R_{sp} is the sheet resistance of the emitter layer (in Ω/square); ρ_{cf} and ρ_{cr} are the contact resistances (in Ω/cm^2) of the front and rear contact, respectively; ρ_b is the base resistivity; and ρ_m is the resistivity of the front metallization. The geometrical dimensions are defined in Fig. 15

Component of resistance	Notation	Expression
Emitter resistance	R_e	$R_e = \frac{R_{sp} d_f}{7\ell_f}$
Resistance of the base	R_b	$R_b = A W_b \rho_b$
Contact resistance: front contact	R_{fc}	$R_{fc} = \frac{\sqrt{R_{sp}\rho d}}{\ell_f} \coth\left(W_f \sqrt{\frac{R_{sp}}{\rho_{cf}}}\right)$
Contact resistance: rear contact	R_{bc}	$R_{bc} = A\rho_{cr}$
Resistance of the finger contact	R_f	$R_f = \frac{\ell_f \rho_m}{3 t_f W_f}$
Resistance of the collecting bus bar (per unit length)	R_{bb}	$R_{bb} = \frac{\rho_m}{3 t_f W_{bb}}$

the two charge states usually considered in the Shockley–Read–Hall theory [32].

4.4 Series resistance

Considerations regarding series resistance form an important part of the solar cell design. The main components of the series resistance of a typical crystalline silicon solar cell are shown in Fig. 15 and expressions are given in Table 2.

REFERENCES

[1] S.M. Sze, Physics of Semiconductor Devices, second ed., John Wiley & Sons, New York, 1981.

[2] Y. Hishikawa, Y. Imura, T. Oshiro, Irradiance dependence and translation of the I–V characteristics of crystalline silicon solar cells, Proc. 28th IEEE Photovoltaic Specialists Conf., Anchorage, 2000, pp. 1464–1467.

[3] J.E. Philips, J. Titus, D. Hofmann, Determining the voltage dependence of the light generated current in $CuInSe_2$-based solar cells using I–V measurements made at different light intensities, Proc. 26th IEEE Photovoltaic Specialist Conf., Anaheim, 1997, pp. 463–466.

[4] S.S. Hegedus, Current-voltage analysis of a-Si and a-SiGe solar cells including voltage-dependent photocurrent collection, Prog. Photovolt. Res. Appl. 5 (1997) 151–168.

[5] M.A. Green, Silicon Solar Cells: Advanced Principles and Practice, Centre for Photovoltaic Devices and Systems, University of New South Wales, Australia, 1995.
[6] L. Castañer, S. Silvestre, Modelling Photovoltaic Systems Using Pspice, John Wiley & Sons, Chichester, 2002.
[7] M. Born, E. Wolf, Principles of Optics, seventh ed., Cambridge University Press, Cambridge, 1999Section 1.6.
[8] K. Zweibel, P. Hersch, Basic Photovoltaic Principles and Methods, Van Nostrand Reinhold, New York, 1984.
[9] A. Goetzberger, J. Knobloch, B. Voss, Crystalline Silicon Solar Cells, John Wiley & Sons, Chichester, 1998.
[10] R. Brendel, H.J. Queisser, On the thickness dependence of open circuit voltages of p–n junction solar cells, Sol. Energy Mater. Sol. Cells 29 (1993) 397.
[11] T. Markvart, Light harvesting for quantum solar energy conversion, Prog. Quantum Electron. 24 (2000) 107.
[12] E. Yablonovich, Statistical ray optics, J. Opt. Soc. Am. 72 (1982) 899.
[13] E. Yablonovich, G.C. Cody, Intensity enhancement in textured optical sheets for solar cells, IEEE Trans. Electron Dev. ED 29 (1982) 300.
[14] J.C. Miñano, Optical confinement in photovoltaics, in: A. Luque, G.L. Araujo (Eds.), Physical Limitations to Photovoltaic Energy Conversion, Adam Hilger, Bristol, 1990, p. 50.
[15] R. Schropp, M. Zeman, Amorphous and Microcystalline Silicon Solar Cells: Modelling, Materials and Device Technology, Kluwer, Boston, 1998.
[16] S. Selberherr, Analysis and Simulation of Semiconductors Devices, Springer, Vienna, New York, 1984, pp. 141–146.
[17] C.T. Sah, R.N. Noyce, W. Shockley, Carrier generation and recombination in p–n junctions and p–n junction characteristics, Proc. IRE 45 (1957) 1228.
[18] D.T. Rover, P.A. Basore, G.M. Thorson, Proc. 18th IEEE Photovoltaic Specialist Conf., Las Vegas, 1985, pp. 703–709.
[19] A. Cuevas, M. Balbuena, Review of analytical models for the study of highly doped regions of silicon devices, IEEE Trans. Electron Dev. ED 31 (1989) 553–560.
[20] M.A. Shibib, F.A. Lindholm, F. Therez, IEEE Trans, Electron Dev. ED 26 (1978) 958.
[21] J.A. del Alamo, R.M. Swanson, Proc. 17th IEEE Photovoltaic Specialist Conf., Orlando, 1984, pp. 1303–1308.
[22] J.S. Park, A. Neugroschel, F.A. Lindholm, IEEE Trans. Electron Dev. ED 33 (1986) 240.
[23] N. Rinaldi, Modelling of minority carrier transport in non-uniformly doped silicon regions with asymptotic expansions, IEEE Trans. Electron Dev. ED 40 (1993) 2307–2317.
[24] R. Alcubilla, J. Pons, L. Castañer, Superposition solution for minority carrier current in the emitter of bipolar devices, Solid State Electron 35 (1992) 529–533.
[25] A. Cuevas, R. Merchan, J.C. Ramos, On the systematic analytical solutions for minority carrier transport in non-uniform doped semiconductors: application to solar cells, IEEE Trans. Electron Dev. ED 40 (1993) 1181–1183.
[26] J.A. del Alamo, R.M. Swanson, The physics and modelling of heavily doped emitters, IEEE Trans. Electron Dev. ED 31 (1984) 1878.
[27] F.J. Bisschop, L.A. Verhoef, W.C. Sinke, An analytical solution for the collection efficiency of solar cell emitters with arbitrary doping profile, IEEE Trans. Electron Dev. ED 37 (1990) 358–364.
[28] L.J. Brillson, Surfaces and interfaces: atomic-scale structure, band bending and band offsets, in: P.T. Landsberg (Ed.), Handbook of Semiconductors, 1, Elsevier, Amsterdam, 1992, pp. 281–417.

[29] R.L. Anderson, Experiments on Ge−As heterojunctions, Solid State Electron 5 (1962) 341−351.
[30] H. Kroemer, Heterostructure devices: a device physicist looks at interfaces, Surf. Sci. 132 (1983) 543−576.
[31] R.S. Crandall, Modelling of thin film solar cells: uniform field approximation, J. Appl. Phys. 54 (1983) 7176.
[32] J. Hubin, A.V. Shah, Effect of the recombination function on the collection in a p−i−n solar cell, Philos. Mag. B72 (1995) 589.
[33] R. van Overstraeten, R.P. Mertens, Physics, Technology and Use of Photovoltaics, Adam Hilger, Bristol, 1986.